Chapter 2

Wind Turbine Modeling

This chapter describes the details of wind turbine modeling. First, a wind energy conversion system is discussed briefly. Then, the modeling and topological overview are presented for both fixed and variable speed wind turbine generator systems. The details of drive train modeling of a fixed speed WTGS are discussed and a six-mass to two-mass conversion method is also presented. Finally, a comparative study is carried out among six-mass, three-mass, and two-mass drive train models.

2.1 Wind Power Output

Gathering or harvesting the wind has been of concern to humans for a long time. Wind turbines have been used for several centuries and literally millions of units have been put into service. For the most part, these machines performed their intended purpose well and in many cases were still being used with minimum maintenance after a half century of service.

Today, wind turbines have to compete with many other energy sources. Therefore, it is important that they should be cost effective. They need to meet any load requirements and produce energy at a minimum cost per dollar of investment. Performance characteristics such as power output versus wind speed or versus rotor angular velocity must be optimized to compete with other energy sources. Yearly energy production and its variation with annual wind statistics must be well known. The shaft torque must be known so that the shaft can be built with adequate strength and the turbine load is properly sized. The output power from ideal and practical wind turbines is discussed in the following two sections [116].

2.1.1 Power Output from an Ideal Turbine

The kinetic energy in a parcel of air of mass, m, flowing at speed, v_w in the x direction is:

$$U = \frac{1}{2} m v_w^{\,2} = \frac{1}{2} (\rho A x) v_w^{\,2} \tag{2.1}$$

where, U is the kinetic energy in joule, A is the cross-sectional area in m^2, ρ is the air density in kg/m^3, and x is the thickness of the parcel in m. If we visualize the parcel as in Fig. 2.1 with side, x, moving at speed, v_w (m/sec), and the opposite side fixed at the origin, we see the kinetic energy increasing uniformly with x, because the mass is increasing uniformly.

The power in the wind, P_w, is the time derivative of the kinetic energy:

$$P_w = \frac{dU}{dt} = \frac{1}{2} \rho A v_w^{\,2} \frac{dx}{dt} = \frac{1}{2} \rho A v_w^{\,3} \tag{2.2}$$

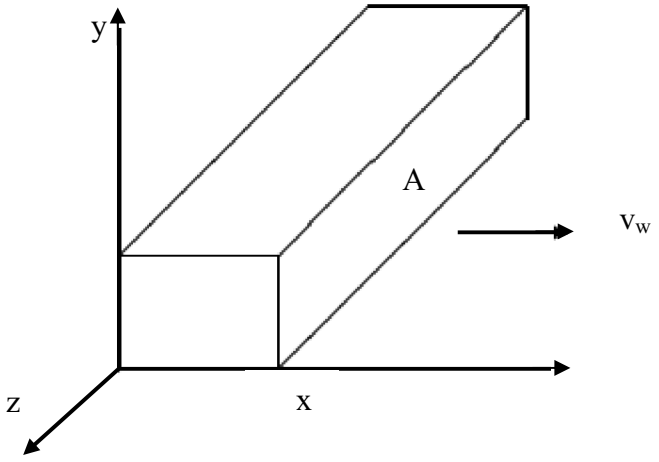

Fig. 2.1 Packet of air moving at speed, v_w [116]

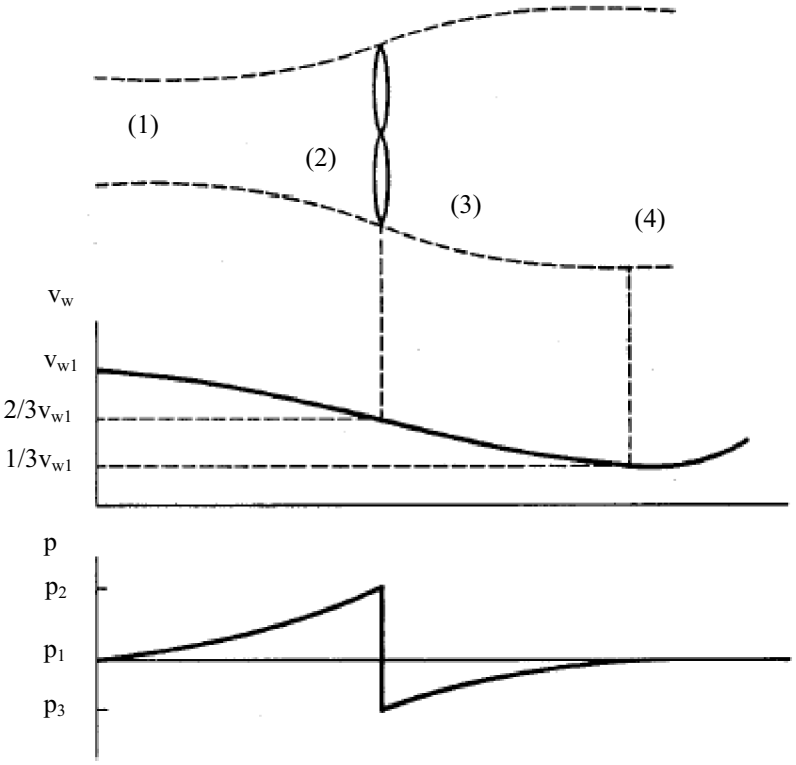

Fig. 2.2 Circular tube of air flowing through an ideal wind turbine [116]

This can be viewed as the power being supplied at the origin to cause the energy of the parcel to increase according to Eq. 2.1. A wind turbine will extract power from side, x, with Eq. 2.2 representing the total power available at this surface for possible extraction.

The physical presence of a wind turbine in a large moving air mass modifies the local air speed and pressure, as shown in Fig. 2.2. The picture is drawn for a conventional horizontal axis propeller type turbine.

Consider a tube of moving air with initial or undisturbed diameter, d_1, speed, v_{w1}, and pressure, p_1, as it approaches the turbine. The speed of the air decreases as the turbine is approached, causing the tube of air to enlarge to the turbine diameter, d_2. The air pressure will rise to the maximum just in front of the turbine and will drop below atmospheric pressure behind the turbine. Part of the kinetic energy in the air is converted to potential energy to produce this increase in pres-

sure. Still more kinetic energy will be converted to potential energy after the turbine, to raise the air pressure back to atmospheric. This causes the wind speed to continue to decrease until the pressure is in equilibrium. Once the low point of wind speed is reached, the speed of the tube of air will increase back to $v_{w4} = v_{w1}$ as it receives kinetic energy from the surrounding air [117].

It can be shown [118] that under optimum conditions, when the maximum power is being transferred from the tube of air to the turbine, the following relationships hold:

$$\left.\begin{aligned} v_{w2} &= v_{w3} = \frac{2}{3} v_{w1} \\ v_{w4} &= \frac{1}{3} v_{w1} \\ A_2 &= A_3 = \frac{3}{2} A_1 \\ A_4 &= 3A_1 \end{aligned}\right\} \tag{2.3}$$

The mechanical power extracted is then the difference between the input and output power in the wind:

$$P_{m,ideal} = P_1 - P_4 = \frac{1}{2}\rho(A_1 v_{w1}^3 - A_4 v_{w4}^3) = \frac{1}{2}\rho(\frac{8}{9} A_1 v_{w1}^3) \tag{2.4}$$

This states that 8/9 of the power in the original tube of air is extracted by an ideal turbine. This tube is smaller than the turbine, however, and this can lead to confusing results. The normal method of expressing this extracted power is in terms of the undisturbed wind speed, v_{w1}, and the turbine area, A_2. This method yields

$$P_{m,ideal} = \frac{1}{2}\rho\left[\frac{8}{9}\left(\frac{2}{3} A_2\right) v_{w1}^3\right] = \frac{1}{2}\rho\left(\frac{16}{27} A_2 v_{w1}^3\right) \tag{2.5}$$

The factor 16/27 = 0.593 is called the Betz coefficient. It shows that an actual turbine cannot extract more than 59.3 percent of the power in an undisturbed tube of air of the same area. In practice, the fraction of power extracted will always be less because of mechanical imperfections. A good fraction is 35 – 40 % of the power in the wind under optimum conditions, although fractions as high as 50 %

have been claimed. A turbine extracts 40 % of the power in the wind, is extracting about two-thirds of the amount that would be extracted by an ideal turbine. This is rather good, considering the aerodynamic problems of constantly changing wind speed and direction as well as the frictional loss due to blade surface roughness.

2.1.2 Power Output from Practical Turbines

The fraction of power extracted from the power in the wind by a practical wind turbine is usually given by the symbol Cp, standing for the coefficient of performance or power coefficient. Using this notation and dropping the subscripts of Eq. 2.5, the actual mechanical power output can be written as

$$P_m = C_p\left(\frac{1}{2}\rho A v_w^{\,3}\right) = \frac{1}{2}\rho\pi R^2 v_w^{\,3} C_p(\lambda,\beta) \tag{2.6}$$

where, R is the blade radius of the wind turbine (m), V_w is the wind speed (m/sec), and ρ is the air density (kg/m^3). The coefficient of performance is not constant, but varies with the wind speed, the rotational speed of the turbine, and turbine blade parameters such as angle of attack and pitch angle. Generally, it is said that power coefficient, Cp, is a function of tip speed ratio, λ, and blade pitch angle, β (deg). The tip speed ratio is defined as

$$\lambda = \frac{\omega_R R}{v_w} \tag{2.7}$$

where, ω_R is the mechanical angular velocity of the turbine rotor in rad/s, and V_w is the wind speed in m/s. The angular velocity ω_R is determined from the rotational speed, n (r/min) by the equation

$$\omega_R = \frac{2\pi n}{60} \tag{2.8}$$

2.2 Wind Turbine Generator System (WTGS)

A wind turbine generator system (WTGS) transforms the energy present in the blowing wind into electrical energy. As wind is highly variable resource that cannot be stored, operation of a WTGS must be done according to this feature. The general scheme of a WTGS is shown in Fig. 2.3.

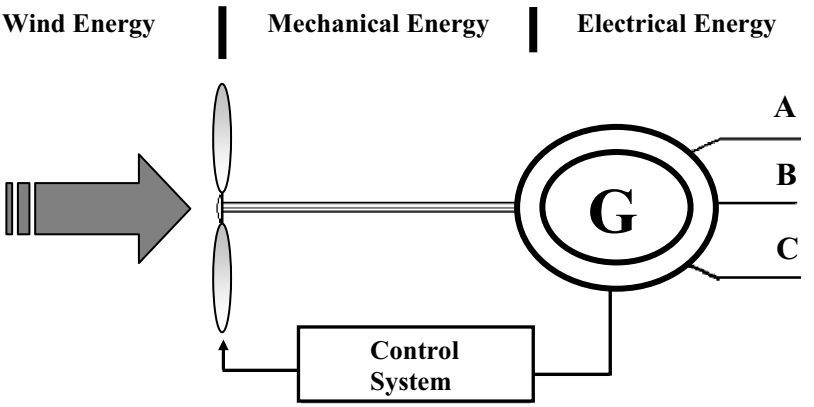

Fig. 2.3 General scheme of a WTGS where three types of energy states are presented: wind, mechanical, and electrical

A short overview of the system is given next. Wind energy is transformed into mechanical energy by a wind turbine that has several blades. It usually includes a gearbox that matches the turbine low speed to the higher speed of the generator. Some turbines include a blade pitch angle control (explained in Chap. 3) for controlling the amount of power to be transformed. Wind speed is measured with an anemometer.

The electrical generator transforms mechanical energy into electrical energy. Commercially available wind generators installed at present are squirrel cage induction generator, doubly fed induction generator, wound field synchronous generator (WFSG), and permanent magnet synchronous generator (PMSG). Based on rotational speed, in general, the wind turbine generator systems can be split into two types:

- Fixed speed WTGS
- Variable speed WTGS

2.3 Fixed Speed WTGS

A fixed speed WTGS consists of a conventional, directly grid coupled squirrel cage induction generator, which has some superior characteristics such as brushless and rugged construction, low cost, maintenance free, and operational simplicity. The slip and hence the rotor speed of a squirrel cage induction generator varies with the amount of power generated. These rotor speed variations are, however, very small, approximately 1 to 2 % of the rated speed. Therefore, this type of wind energy conversion system is normally referred to as a constant or fixed speed WTGS. The advantage of a constant speed system is that it is relatively simple. Therefore, the list price of constant speed turbines tends to be lower than that of variable speed turbines. However, constant speed turbines must be more mechanically robust than variable speed turbines [119]. Because the rotor speed cannot be varied, fluctuations in wind speed translate directly into drive train torque fluctuations, causing higher structural loads than with variable speed operation. This partly cancels the cost reduction achieved by using a relatively cheap generating system.

2.3.1 Fixed Speed WTGS Topology

The fixed speed WTGS topology is shown in Fig. 2.4. In the fixed speed WTGS topology, both single and double cage squirrel cage induction generators are commercially used. Note that squirrel cage induction generators used in wind turbines can often run at two different (but constant) speeds by changing the number of pole pairs of the stator winding. The relation between pole pairs and rotational speed is as follows:

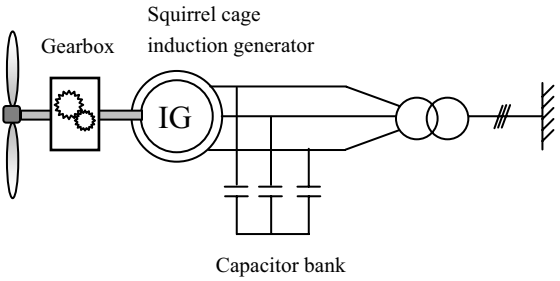

Fig. 2.4 Schematic diagram of a fixed speed WTGS

$$\omega_s = \frac{120f}{p} \tag{2.9}$$

where, f is the frequency of the stator voltage, p is the number of pole pairs, and ω_s is the generator rotor speed (rpm). There is a big speed difference between the turbine hub and the squirrel cage induction generator. Therefore, a gearbox is used in this topology that matches the turbine low speed to the higher speed of the generator.

A squirrel cage induction generator has a principal characteristic that it always consumes reactive power. To establish the rotating magnetic field of the stator, reactive power must be supplied from the network to the stator winding of the induction generator. In most cases, this is undesirable, particularly for large turbines and weak grids. Therefore, the reactive power consumption of the squirrel cage induction generator is nearly always partly or fully compensated by a capacitor bank to achieve a power factor close to one in the steady state. As a result, during load flow calculation this reactive power, Q_C, supplied by the capacitor bank should be considered. Figure 2.5 shows the schematic diagram of the entire power system including a wind turbine generator system (WTGS) that can be used for load flow study.

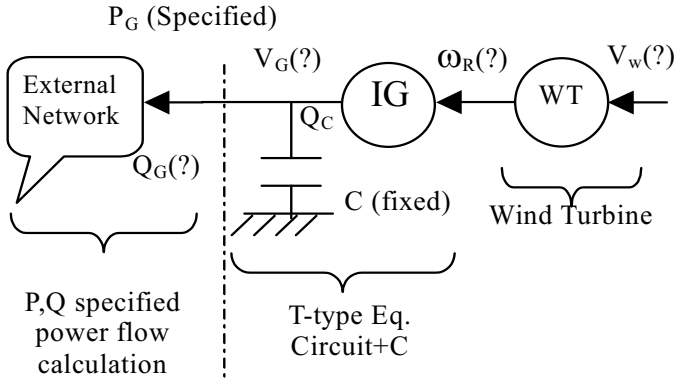

Fig. 2.5 Initial value calculation for a grid connected WTGS

The flowchart for determining the initial values of a WTGS connected to an external network is shown in Fig. 2.6. First, it is assumed that real power, P_G, and reactive power, Q_G, (initially zero) at the terminal of the IG are specified. By using these specified values, the entire power flow calculation should be done. Then a

particular terminal voltage, V_G, is obtained. Next, the WTGS-SUBROUTINE, which also includes wind turbine characteristic, is called. Here, for specified V_G and P_G, wind speed, V_W, and slip, s, of the induction generator are determined from which the IG rotor speed, ω_R, can be calculated easily. Q_G is also determined within this subroutine. At this stage, the convergence of Q_G is checked. If Q_G does not converge, then the power flow calculation must be continued as shown in Fig. 2.6.

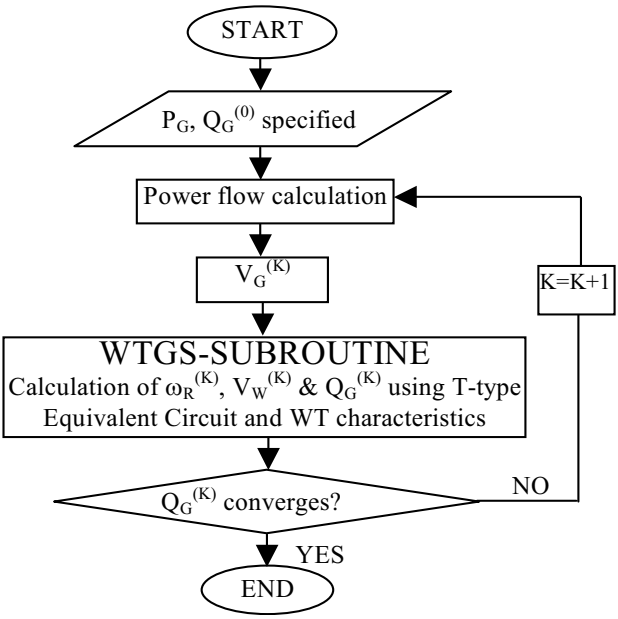

Fig. 2.6 Flowchart for power flow calculation including a WTGS

2.3.1.1 Equivalent Circuit Analysis

Both single and double cage induction generators are used as fixed-speed wind generators. The equivalent circuits of single and double cage induction generators are shown in Figs. 2.7 and 2.8, respectively, where s denotes rotational slip. From the single cage equivalent circuit of an IG shown in Fig. 2.7, the loop equations can be derived as Eqs. 2.10 and 2.11. From these two equations we can obtain the desired currents i_1 and i_2. Again, from the equivalent circuit of a single cage IG,

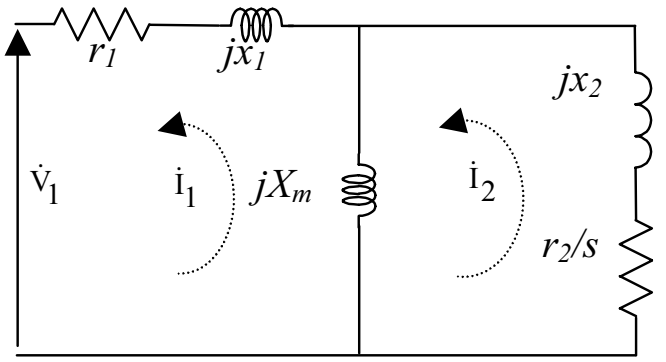

Fig. 2.7 Equivalent circuit of a single cage induction generator

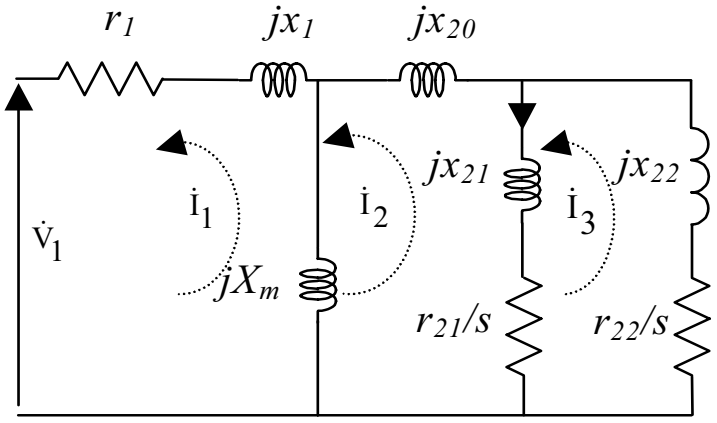

Fig. 2.8 Equivalent circuit of a double cage induction generator

we can calculate the input power of the induction generator, $P_{IG\_IN\_SINGLE}$, which is actually the output power of the wind turbine, shown in Eq. 2.12. From double cage equivalent circuit of the induction generator shown in Fig. 2.8, the loop equations can be derived as Eqs. 2.10, 2.13, and 2.14. From these three equations we can get the desired currents $\dot{i}_1$, $\dot{i}_2$, and $\dot{i}_3$. From the equivalent circuit of the double cage induction generator, we can calculate the input power of induction generator, $P_{IG\_IN\_DOUBLE}$, shown in Eq. 2.15. We can also calculate the desired output

power of both single and double cage induction generators, P_{IG_OUT}, shown in Eq. 2.16, from the equivalent circuits shown in Figs. 2.7 and 2.8. The detailed description of the WTGS subroutine is presented below, in the light of the single cage equivalent circuit of the induction generator [43,108].

$$\dot{V}_1 = -(r_1 + jx_1 + jx_m)\dot{I}_1 + jx_m\dot{I}_2 \tag{2.10}$$

$$0 = jx_m\dot{I}_1 - (\frac{r_2}{s} + jx_2 + jx_m)\dot{I}_2 \tag{2.11}$$

$$P_{IG\_IN\_SINGLE} = I_2^{\,2}\,\frac{(1-s)}{s}\,r_2 \tag{2.12}$$

$$0 = jx_m\dot{I}_1 - (\frac{r_{21}}{s} + jx_{21} + jx_{20} + jx_m)\dot{I}_2 + (\frac{r_{21}}{s} + jx_{21})\dot{I}_3 \tag{2.13}$$

$$0 = (\frac{r_{21}}{s} + jx_{21})\dot{I}_2 - (\frac{r_{21}}{s} + \frac{r_{22}}{s} + jx_{21} + jx_{22})\dot{I}_3 \tag{2.14}$$

$$P_{IG\_IN\_DOUBLE} = I_3^{\,2}\,\frac{(1-s)}{s}\,r_{22} + (I_3 - I_2)^2\,\frac{(1-s)}{s}\,r_{21} \tag{2.15}$$

$$P_{IG\_OUT} = \mathrm{Re}\left[\dot{V}_1\dot{I}_1^{\,*}\right] \tag{2.16}$$

2.3.1.2 WTGS-SUBROUTINE

Two probable cases have been considered for calculating the initial conditions of a wind turbine generator system.

Case I: In this case, it has been considered that the wind speed, V_W, is less than or equal to the rated wind speed. Therefore, the pitch angle, β, is set to zero. In order to get a desired output power from an induction generator, we need to know the exact wind speed. The whole procedure is briefly described in Fig. 2.9. First, we need to set two inputs. One is desired the IG output power, $P_{IG\text{-}OUT}$, and the other is the IG terminal voltage, V_T, that can be obtained from the power flow calculation. The initial values of the wind speed, V_W, and rotor speed, ω_R, are also

needed. Now turbine torque, T_W, can be calculated by dividing the turbine mechanical power, P_m, shown in Eq. 2.6 by the tip speed ratio, λ, for $\beta = 0$.

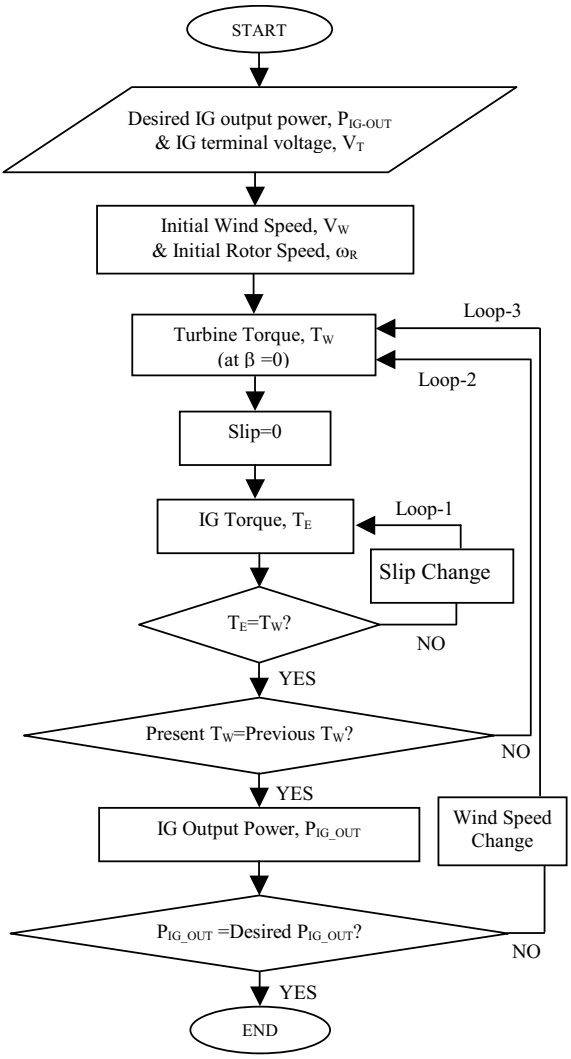

Fig. 2.9 Flowchart for initial value calculation (Case I)

The developed torque, T_E, of the IG can also be calculated from Eq. 2.12. The slip, s, is changed in loop-1 until T_E becomes equal to T_W. Using this slip, the new

rotor speed, ω_R, can be calculated easily and this ω_R is used to calculate the wind turbine torque, T_W, instead of the initial ω_R until the present T_W becomes equal to the previous T_W in loop-2. When these two become equal, the present IG output power, $P_{IG\text{-}OUT}$, is calculated from Eq. 2.16. Loop-3 will be continued by changing the wind speed as shown in Fig. 2.9, until the present $P_{IG\text{-}OUT}$ becomes equal to the desired $P_{IG\text{-}OUT}$. Finally, we will get the desired the wind speed for any particular induction generator output power.

Case II: In this case, it is considered that the wind speed, V_W, is above the rated speed. Therefore, we need to increase the pitch angle, β, to generate the rated induction generator output power. This process has been demonstrated in Fig. 2.10. Here, we assumed that wind speed, V_W, and terminal voltage, V_T, are known. The pitch angle, β, has been set to zero initially, and the rotor speed, ω_R, has also been approximated. Slip searching and the rotor speed determination process, which are already described in Case I, have been shown by dotted lines in Fig. 2.10. For a particular slip, when the present T_W and the previous T_W become equal, the IG output power, $P_{IG\text{-}OUT}$, is calculated. If it exceeds the rated output, then β is increased, and loop-3 will be continued until $P_{IG\text{-}OUT}$ becomes equal to the rated power. Therefore, finally, we will get a particular β for any wind speed over the rated speed, at which the induction generator output power becomes the rated power.

2.3.2 Fixed Speed Wind Turbine Characteristics

The modeling of a wind turbine rotor is somewhat complicated. According to the blade element theory [120], the modeling of blade and shaft needs complicated and lengthy computations. Detailed and accurate information about rotor geometry are also needed. For that reason, considering only the electrical behavior of the system, a simplified method of modeling the wind turbine blade and shaft is normally used.

For fixed speed wind turbine characteristics, the following Cp equations have been used from [33].

$$\lambda = \frac{V_w}{\omega_R} \tag{2.17}$$

$$C_p = \frac{1}{2}(\lambda - 0.022\beta^2 - 5.6)e^{-0.17\lambda} \tag{2.18}$$

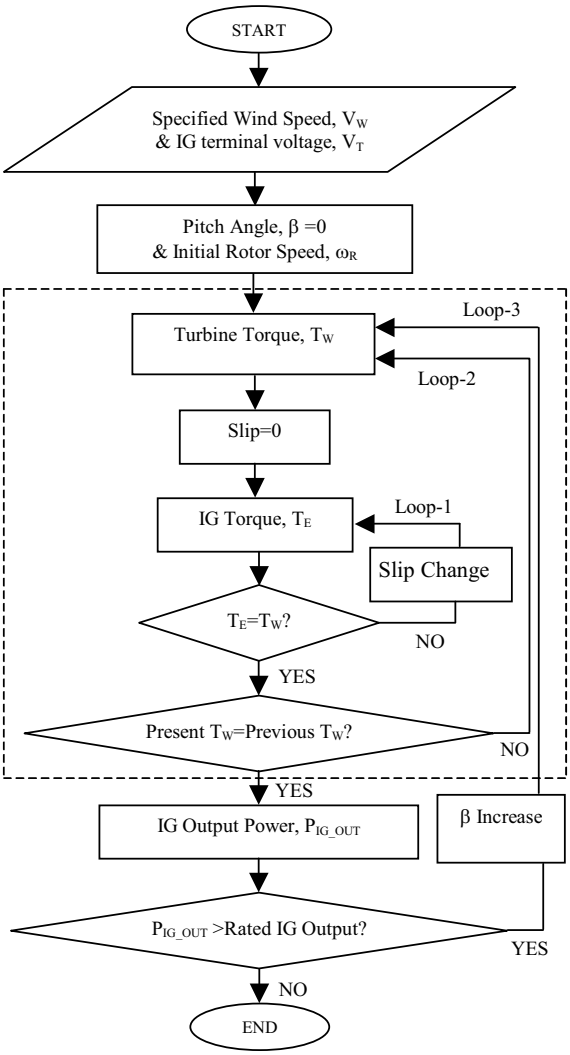

Fig. 2.10 Flowchart for initial value calculation (Case II)

In Eq. 2.17, the wind speed, V_w is in mile/hr. Keeping the original definition of tip speed ratio, λ, in Eq. 2.7, and changing the unit of wind speed from mile/hr to m/sec, Eqs. 2.17 and 2.18 are rearranged as shown below:

$$\lambda_i = \frac{3600R}{1609\lambda} \tag{2.19}$$

$$C_p = \frac{1}{2}(\lambda_i - 0.022\beta^2 - 5.6)e^{-0.17\lambda_i} \quad (2.20)$$

The Cp-λ curves for MOD2 wind turbine [33] are shown in Fig. 2.11 for different values of β. Power versus wind speed and pitch angle versus wind speed curves are shown together in Fig. 2.12.

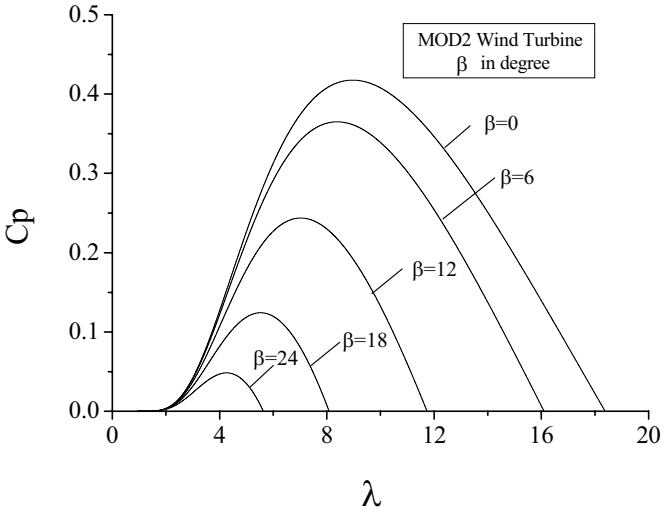

Fig. 2.11 C_P- λ curves for different pitch angles

2.3.3. Drive Train Modeling

The following four types of drive train models of the WTGS are usually available in the power system analysis:

- Six-mass drive train model
- Three-mass drive train model
- Two-mass shaft model
- One-mass or lumped model

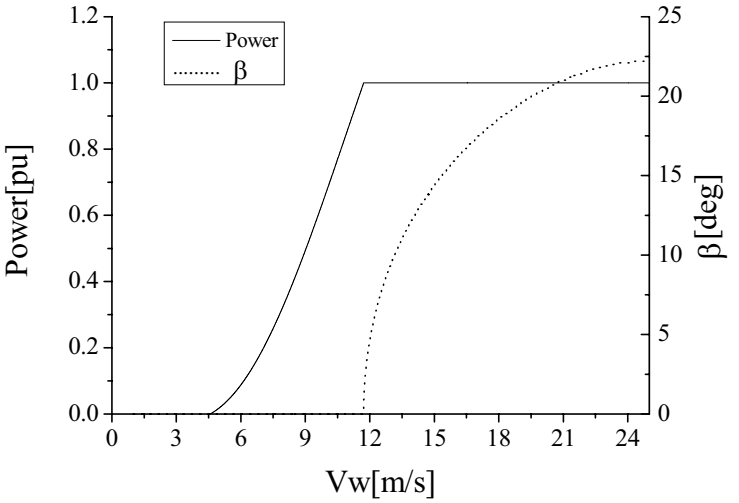

Fig. 2.12 Power vs. wind speed and pitch angle vs. wind speed characteristics

Figures 2.13a, b, d, and e show the above-mentioned six-mass, three-mass, two-mass, and one-mass drive train models, respectively. In the following few sections, the transformed three-mass drive train model shown in Fig. 2.13c is explained.

2.3.3.1 Six-Mass Drive Train Model

The basic six-mass drive train model is presented in Fig. 2.13a. The six-mass model system has six inertias: three blade inertias (J_{B1}, J_{B2}, and J_{B3}), hub inertia, J_H, gearbox inertia, J_{GB}, and generator inertia, J_G. θ_{B1}, θ_{B2}, θ_{B3}, θ_H, θ_{GB}, and θ_G represent angular positions of the blades, hub, gearbox and generator. ω_{B1}, ω_{B2}, ω_{B3}, ω_H, ω_{GB}, and ω_G correspond to the angular velocities of the blades, hub, gearbox, and generator. The elasticity between adjacent masses is expressed by the spring constants K_{HB1}, K_{HB2}, K_{HB3}, K_{HGB}, and K_{GBG}. The mutual damping between adjacent masses is expressed by d_{HB1}, d_{HB2}, d_{HB3}, d_{HGB}, and d_{GBG}. There exist some torque losses through external damping elements of individual masses, represented by D_{B1}, D_{B2}, D_{B3}, D_H, D_{GB}, and D_G. The model system needs generator torque, T_E and three individual aerodynamic torques acting on each blade (T_{B1},T_{B2}, and T_{B3}). The sum of the blade torques is the turbine torque, T_{WT}. It is assumed that the aerodynamic torques acting on the hub and gearbox are zero.

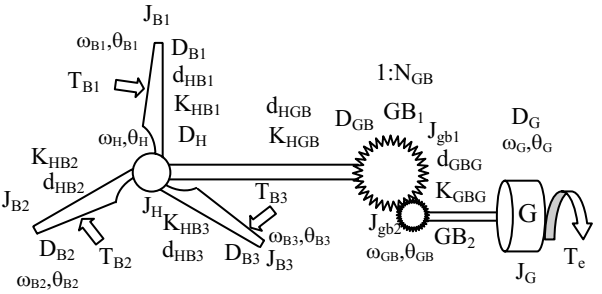

(a) Six-mass model

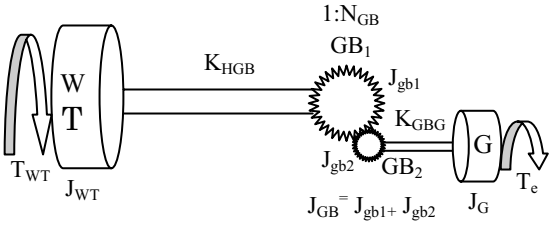

(b) Three-mass model

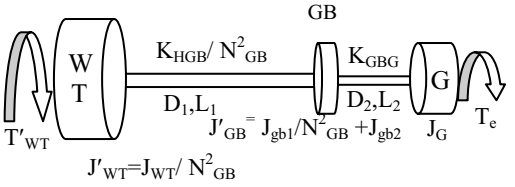

(c) Transformed three-mass system

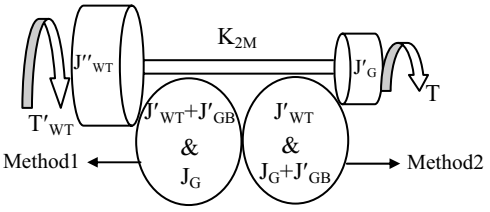

(d) Two-mass shaft model

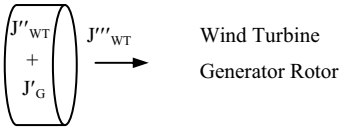

(e) One-mass or lumped model

Fig. 2.13 Drive train models of wind turbine generator systems

2.3.3.2 Three-Mass Drive Train Model

The basic three-mass model is shown in Fig. 2.13b. The turbine inertia can be calculated from the combined weight of the three blades and hub. Therefore, the mutual damping between the hub and the blades is ignored in the three-mass model. Individual blade torque sharing cannot be considered in this model. Instead, it is assumed that the three-blade turbine has uniform weight distribution for simplicity, i.e., the turbine torque, T_{WT}, is assumed to be equal to the sum of the torque acting on the three blades. Therefore, the turbine can be looked upon as a large disk with small thickness. If proper data are not available, the simple equation below can be used for estimating the mass moment of inertia of a disk with small thickness [121].

$$J(\mathrm{Kg.m}^2) = \frac{MD_d^2}{8} \tag{2.21}$$

where, D_d is the diameter of the disk and M is the weight of the disk. Similarly, generator and gearbox inertia can be calculated approximately from their diameter and weight. If we need precise estimation, precise data of geometry and very complicated formulas are needed for calculating the moment of inertia of the turbine, gearbox, and generator.

The shaft stiffness can be calculated from the equation below [122]:

$$K(\mathrm{Nm/rad}) = \frac{G\pi D_{sh}^4}{32L} \tag{2.22}$$

where, D_{sh} is the shaft diameter, L is the shaft length, and G is the shear modulus. Stainless steel or ductile cast iron is normally used as the shaft material.

2.3.3.3 Geared System Transformation

When a torsional system is interconnected by a set of gears, the inertia disks are not being operated at the same angular speed throughout the system. In that case, the actual system needs to be corrected for the differences in the speeds of the component parts, i.e., the inertias and spring constants are referred to one speed of rotation, as shown in Fig. 2.13c. The basis for these transformations is that the potential and kinetic energies of the equivalent system should be the same as those of the actual one, and it is assumed that the gear teeth do not break contact while transmitting vibration. The above-mentioned transformation can be summarized as follows [122, 123]:

$$\frac{J_{eq}}{J_a} = \frac{K_{eq}}{K_a} = (\text{speed ratio})^2 \tag{2.23}$$

where, the suffixes ‘eq’ and ‘a’ means equivalent and actual, respectively.

2.3.3.4 Two-Mass Drive Train Model

The three-mass system can be converted into a two-mass system, which is shown in Fig. 2.13d by adding the masses of two disks together and by connecting the two disks with equivalent shaft stiffness. The equivalent shaft stiffness of the two-mass system, K_{2M}, can be determined from the parallel shaft stiffness as in Eq. 2.24 [122, 123]. In Fig. 2.13d, J''_{WT} and J'_G represent the equivalent mass moments of inertia of the wind turbine and generator, respectively.

Note here that the two disks should be added together by considering the lower shaft stiffness. For example, if the spring constant of the low-speed side is lower than that of the high-speed side, then the gearbox and generator inertias should be added, as shown in method-2 of Fig. 2.13d and vice versa, which can be ensured from the simulation results presented in Sect. 2.3.4.3.1. This might be a good practice for wind turbine drive train conversion methodology instead of the conventional one of connecting the turbine and gearbox together, as presented in [26]. Accordingly, the self damping of the generator and gearbox should be added together and the mutual damping of the gearbox and generator is neglected in the two-mass shaft model:

$$\frac{1}{K_{2M}} = \frac{1}{K_{HGB}/N_{GB}^2} + \frac{1}{K_{GBG}} \tag{2.24}$$

2.3.3.5 One-Mass Lumped Model

In the one-mass or lumped model, all types of windmill drive train components are lumped together and work as a single rotating mass, as shown in Fig. 2.13e. The dynamic behavior can be expressed by the following differential equation:

$$\frac{d\omega_R}{dt} = \frac{T_{WT} - T_E}{J'''_{WT}} \tag{2.25}$$

where, J'''_{WT} is the inertia constant of the rotating mass, ω_R is the rotor speed, T_{WT} is the input mechanical torque applied to the wind turbine rotor and T_E is the electromagnetic torque of the induction generator.

2.3.3.6 Per Unitization

In the drive train model system, all data used in the state equations are converted to a per unit system. If P_B is the base power (VA), ω_0 the base electrical angular velocity (rad/sec) and P the number of pole pairs of the generator, the base values of the per unit system at the high-speed side of the drive train are defined as follows:

The base mechanical speed (mech. rad/sec), $\omega'_B = \omega_0/P$

The base torque (Nm), $T'_B = P_B/\omega'_B$

The base inertia [Nm/(rad/sec)], $J'_B = \dfrac{T'_B}{0.5\omega'_B} = \dfrac{P_B}{0.5\omega'^2_B}$

The base spring constant, [Nm/(rad/sec)], $K'_B = \dfrac{T'_B}{\omega'_B} = \dfrac{P_B}{\omega'^2_B}$

The base damping constant, [Nm/(rad/sec)], $D'_B = d'_B = \dfrac{T_B}{\omega'_B} = \dfrac{P_B}{\omega'^2_B}$

Now, the low-speed side (turbine-side) base quantities can be calculated from the high-speed side (generator-side) base quantities using the gearbox speed ratio, N_{GB}, as follows:

$$\begin{aligned} \omega''_B &= \omega'_B / N_{GB} & J''_B &= N^2_{GB} J'_B \\ \theta''_B &= \theta'_B / N_{GB} & D''_B &= N^2_{GB} D'_B \\ T''_B &= N_{GB} T'_B & K''_B &= N^2_{GB} K'_B \end{aligned} \tag{2.26}$$

In the simulation study, $H_{B\,(1,2,3)}$, H_H, H_{GB}, and H_G represent the per unit inertia constants (sec) of three blades, hub, gearbox, and generator, respectively.

2.3.3.7 Wind Farm Equivalent n-Machine

For the transient stability analysis of a WTGS, it is cumbersome to simulate each individual wind turbine. Therefore, wind turbines with the same torsional natural frequency might be added as follows [12, 27]:

$$\left.\begin{aligned} J_{wt} &= \sum_{i=1}^{p} J_{wti} \\ J_{gb} &= \sum_{i=1}^{p} J_{gbi} \\ J_{g} &= \sum_{i=1}^{p} J_{gi} \\ K &= \sum_{i=1}^{p} K_{i} \end{aligned}\right\} \tag{2.27}$$

where, i = number of each individual wind turbine and p = total number of wind turbine.

2.3.4 Comparative Study Among Different Types of Drive Train Modeling

2.3.4.1 Simulation Model

Two types of model systems are used for the sake of exact comparison among different types of drive train models of a WTGS. Figure 2.14 shows model system I, where one synchronous generator (SG) is connected to an infinite bus through a transformer and a double circuit transmission line. In the figure, the double circuit transmission line parameters are numerically shown in the form of R+jX, where R and X represent the resistance and reactance, respectively. One wind farm (Induction generator, IG) is connected with the network via a transformer and a short transmission line. A capacitor bank has been used for reactive power compensation at steady state. The value of capacitor C is chosen so that the power factor of the wind power station becomes unity [43] during the rated operation. Automatic voltage regulator (AVR) and governor (GOV) control system models shown in Figs. 2.15 and 2.16, respectively have been included in the synchronous generator model in the simulations. Figure 2.17 shows model system II, where the aggregated model of the wind farm (induction generator) is directly connected to the synchronous generator through a double circuit transmission line.

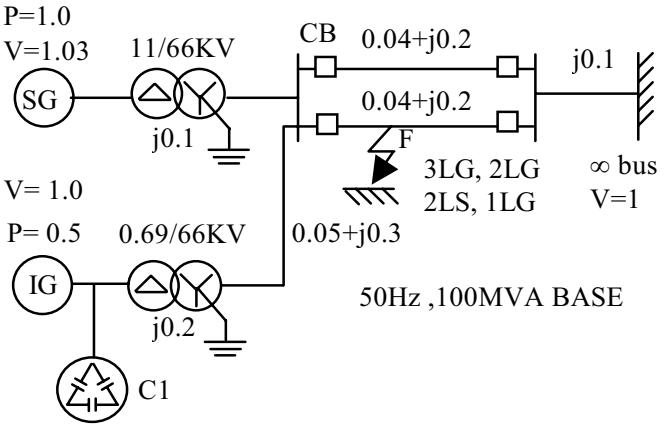

Fig. 2.14 Model system I

The IEEE generic turbine model and approximate mechanical-hydraulic speed governing system are used with a synchronous generator [124]. The IEEE alternator supplied rectifier excitation system (AC1A) [125] is used for excitation control of the synchronous generator. The generator parameters for both model systems are shown in Table 2.1. The initial values used for model systems I and II are shown in Tables 2.2 and 2.3, respectively. The drive train parameters for the six-mass, three-mass, and two-mass models are shown in Tables 2.4 and 2.5. For transient stability analysis, the symmetrical three-line-to-ground fault, 3LG, is considered. Some unsymmetrical faults such as double-line-to-ground fault, 2LG (phases a and b), line-to-line fault, 2LS (between phases a and b), and single-line-to-ground fault, 1LG (phase a) are also considered. Time step and simulation time were chosen 0.00005 sec and 10 sec, respectively. The simulations were done by using PSCAD/EMTDC[1] [126].

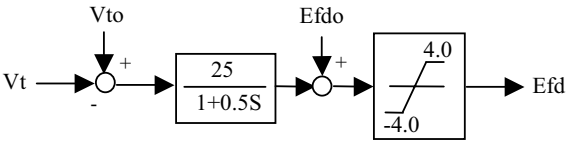

Fig. 2.15 AVR model

[1] For the latest information on PSCAD/EMTDC, visit at http://pscad.com

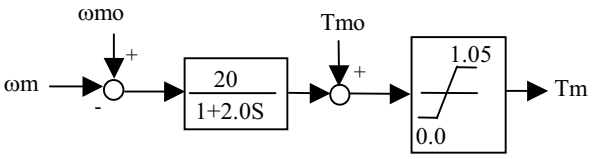

Fig. 2.16 GOV model

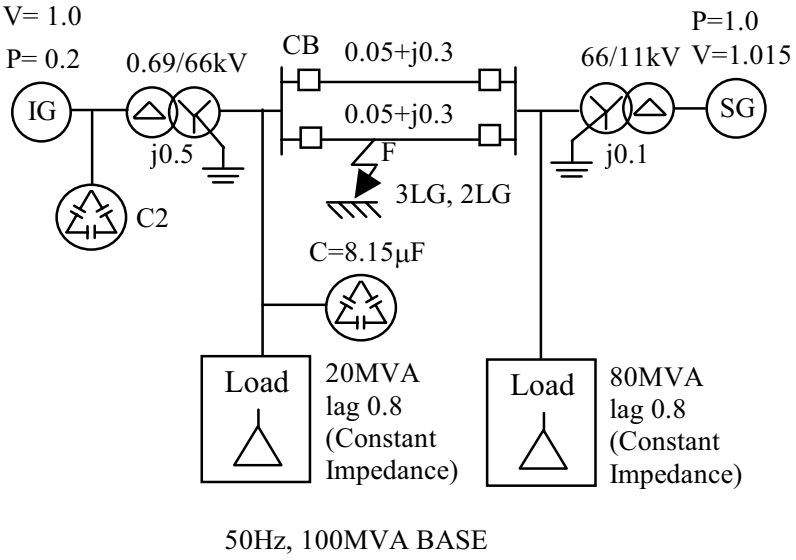

Fig. 2.17 Model system II

2.3.4.2 Effects of Equal and Unequal Blade Torque Sharing on Stability

Wind speed is intermittent and stochastic by nature. Therefore, the torques acting on the three blades of a wind turbine are not always equal. In this section, the effect of equal and unequal torque sharing on transient stability are analyzed using the six-mass drive train model. A 3LG fault is considered to occur at fault point F of model system I. The initial values for the stable and unstable cases are shown as Condition 1 and Condition 2 in Table 2.2. The drive train parameters of the six-mass model are shown in Table 2.4, but all types of damping are disregarded in this case to consider the worst-case scenario.

Table 2.1 Generator parameters

SG		IG	
MVA	100	MVA	50/20
ra (pu)	0.003	r1 (pu)	0.01
xa (pu)	0.13	x1 (pu)	0.1
Xd (pu)	1.2	Xmu (pu)	3.5
Xq (pu)	0.7	r21 (pu)	0.035
Xd' (pu)	0.3	x21 (pu)	0.030
Xq' (pu)	0.22	r22 (pu)	0.014
Xd'' (pu)	0.22	x22 (pu)	0.098
Xq'' (pu)	0.25		
Tdo' (sec)	5.0		
Tdo'' (sec)	0.04		
Tqo'' (sec)	0.05		
H (sec)	2.5		

Table 2.2 Initial conditions of generators and turbines (model system I)

	Condition 1		**Condition 2**		**Condition 3**	
	SG	**IG**	**SG**	**IG**	**SG**	**IG**
P(pu)	1.0	0.39	1.0	0.40	1.0	0.50
V(pu)	1.03	1.042	1.03	1.039	1.03	0.999
Q(pu)	0.244	0.053 (0.206)*	0.251	0.049 (0.209)*	0.334	0.000 (0.239)*
Efd(pu)	1.719	-	1.725	-	1.803	-
Tm(pu)	1.003	-	1.003	-	1.003	-
SG_{δ}(deg)	50.47	-	50.50	-	50.72	-
slip	0.0	–0.769%	0.0	–0.794%	0.0	–1.09%
Vw (m/s)	-	10.615	-	10.722	-	11.797
β (deg)	-	0	-	0	-	0

* Reactive power drawn by an induction generator

Table 2.3 Initial conditions of generators and turbines (model system-II)

	Condition 4		**Condition 5**	
	SG	**IG**	**SG**	**IG**
P(pu)	0.624	0.16	0.58	0.20
V(pu)	1.015	1.014	1.015	1.00
Q(pu)	0.279	0.018 (0.081)*	0.297	0.000 (0.095)*
Efd(pu)	1.50	-	1.50	-
Tm(pu)	0.626	-	0.582	-
slip	0.0	–0.835%	0.0	–1.09%
Vw (m/s)	-	10.74	-	11.79
β (deg)	-	0	-	0

* Reactive power drawn by an induction generator

Table 2.4 Six-mass and three-mass drive train model parameters of a WTGS in per unit (from [32]) [based on high-speed rotation]

	6 M	3 M		6 M	3 M		6 M	3 M
$H_{B(1,2,3)}$	0.6388	-	K_{HGB}	54.75	54.75	D_G	0.01	0.01
H_H	0.0114	-	K_{GBG}	1834.1	1834.1	$d_{HB(1,2,3)}$	12.0	-
H_{WT}	-	1.9277	$D_{B(1,2,3)}$	0.004	-	d_{HGB}	3.5	3.5
H_{GB}	0.0806	0.0806	D_H	0.01	-	d_{GBG}	10.0	10.0
H_G	0.1419	0.1419	D_{WT}	-	0.022			
$K_{HB(1,2,3)}$	1259.8	-	D_{GB}	0.022	0.022			

Table 2.5 Two-mass drive train model parameters of a WTGS in per unit (transformation is based on six-mass drive train parameters)

2M					
H''_{WT}	1.9277	K_{2M}	53.16	D'_G	0.032
H'_G	0.2225	D''_{WT}	0.022	d''_{2M}	3.5

The responses of the IG rotor and turbine hub speeds are shown in Figs. 2.18 and 2.19, respectively, for both stable and unstable situations. It is seen from Figs. 2.18 and 2.19 that unequal blade torque sharing has no effect on the transient stability of a WTGS. Therefore, the three-mass and two-mass reduced order drive train models can be used, where it is assumed that the turbine torque is equal to the sum of the torques acting on the three blades. The comparison among the three types of drive train models of a WTGS during network disturbances is presented in the next section by using model systems I and II.

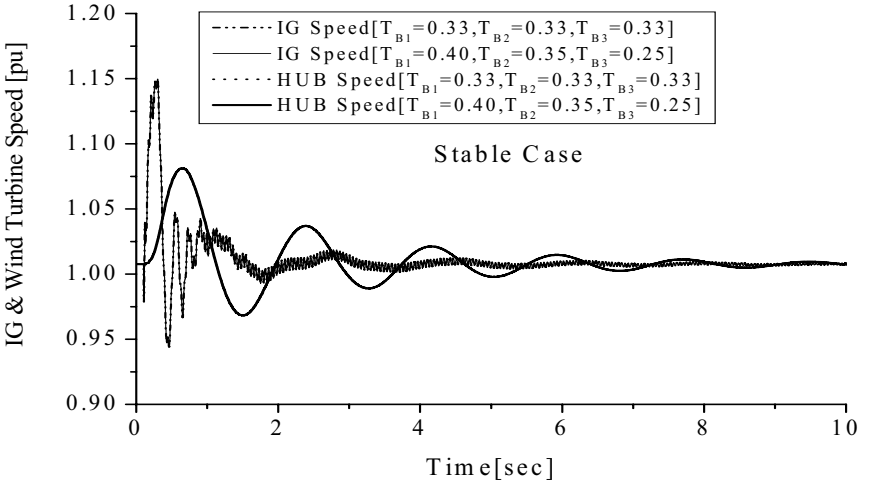

Fig. 2.18 Transient effect of equal and unequal blade torque sharing (Condition 1, 3LG, stable case, model system I)

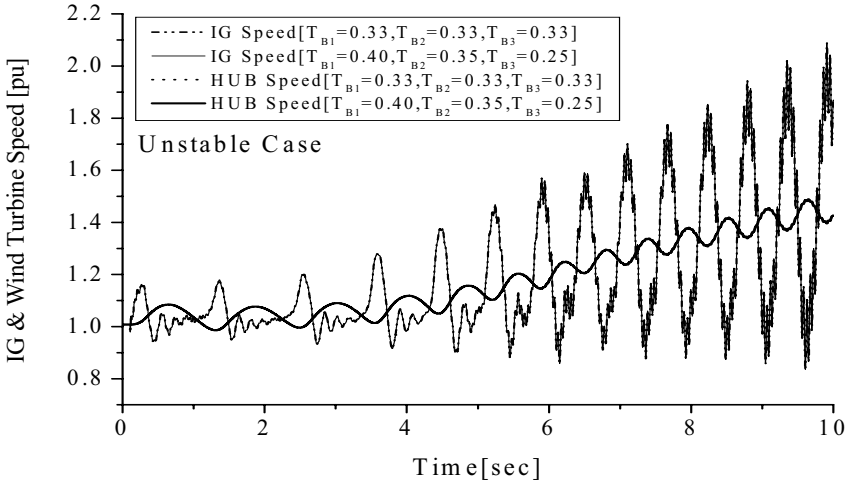

Fig. 2.19 Transient effect of equal and unequal blade torque sharing (Condition 2, 3LG, unstable case, model system I)

2.3.4.3 Comparison Using Model System I

First, the effect of the drive train parameters of the six, three, and two-mass drive train models on the transient stability of a WTGS are analyzed by using model system I. The comparison is carried out at different IG output power levels for different types of symmetrical and unsymmetrical faults. The fault is considered to occur at 0.1 sec, the circuit breakers (CB) on the faulted line are opened at 0.2 sec and at 1.0 sec, are reclosed.

2.3.4.3.1 Effects of Drive Train Parameters on the Transient Stability of WTGS

The effects of the drive train parameters on the transient stability of a grid connected WTGS are analyzed by considering the severe 3LG fault that occurred at point F of Fig. 2.14. The initial values are presented as Condition 2 in Table 2.2.

a. Effect of Inertia Constants

In this sub-section, the effects of inertia constant on the transient stability of a WTGS are analyzed using the six-mass, three-mass, and two-mass drive train models. All types of damping are neglected in this case. For the two-mass shaft model, two types of inertia sets are used, as shown in Fig. 2.13d. Responses of the IG speed and turbine speed are shown in Figs. 2.20 and 2.21, respectively for the six-mass, three-mass, and two-mass drive train models. Some other simulation results of IG rotor and turbine speeds are presented in Figs. 2.22 and 2.23, respectively, where the turbine inertia of each drive train model is increased by 50 % from the original value shown in Tables 2.4 and 2.5. In Figs. 2.24 and 2.25, the IG

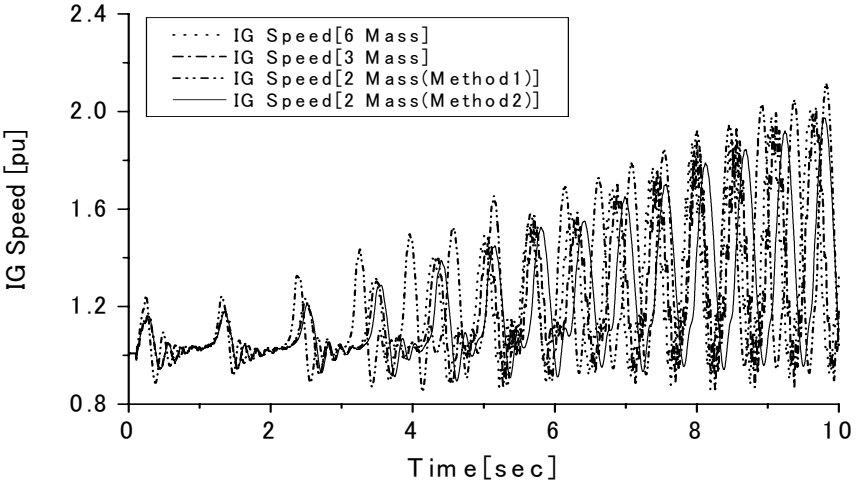

Fig. 2.20 Effect of inertia constant on generator speed (Condition 2, 3LG, model system I)

rotor and turbine speeds are shown, respectively, where the generator inertia constant of each drive train model is increased by about 50 % from the original value shown in Tables 2.4 and 2.5. It is clear from Figs. 2.24 and 2.25 that the transformation from three-mass to two-mass is needed to perform according to method 2 of Fig. 2.13d, i.e., the gearbox and generator masses should be added together as they are separated with comparatively lower shaft stiffness. Moreover, it is seen that the increase of turbine and generator inertia constants enhances the transient stability of the WTGS for all types of drive train models. From Figs. 2.20 – 2.25, it is clear that if the proper transformation process is applied, then the two-mass shaft model shows almost the same transient characteristics as those of the six-mass and three-mass drive train models.

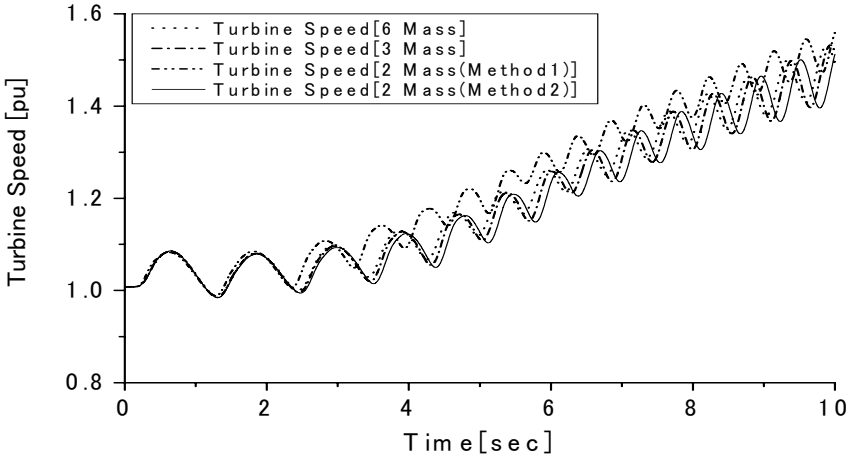

Fig. 2.21 Effect of the inertia constant on the turbine speed (Condition 2, 3LG, model system I)

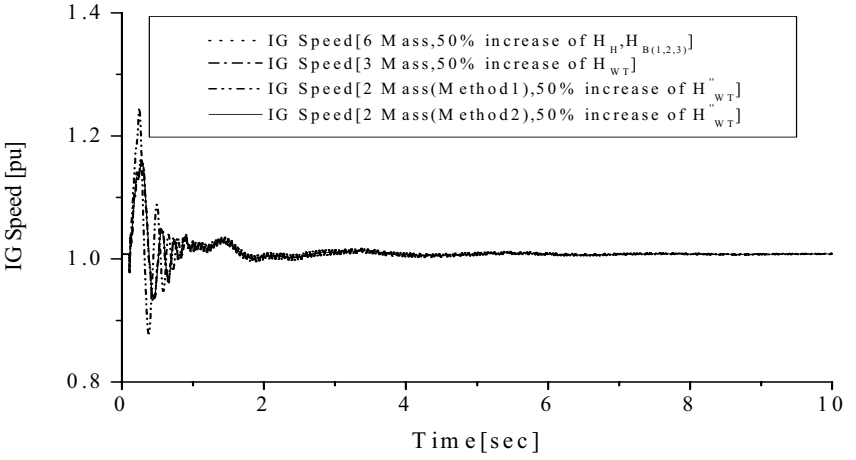

Fig. 2.22 Effect of the increased inertia constant of the turbine on the generator speed (Condition 2, 3LG, model system I)

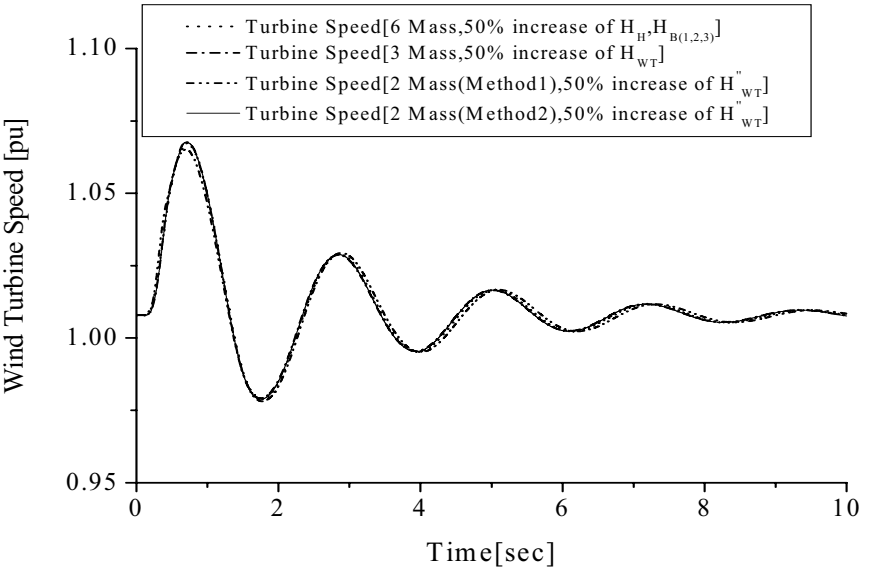

Fig. 2.23 Effect of the increased inertia constant of the turbine on the turbine speed (Condition 2, 3LG, model system I)

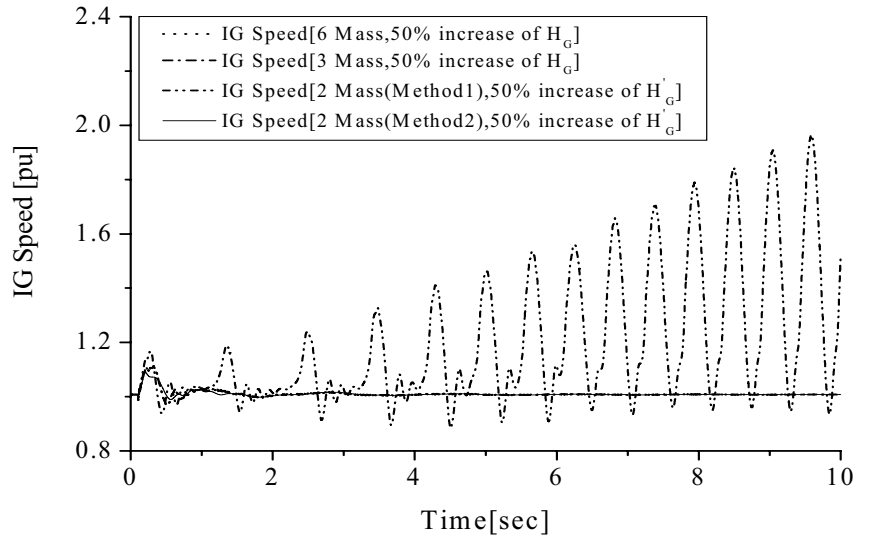

Fig. 2.24 Effect of the increased inertia constant of the generator on its rotor speed (Condition 2, 3LG, model system I)

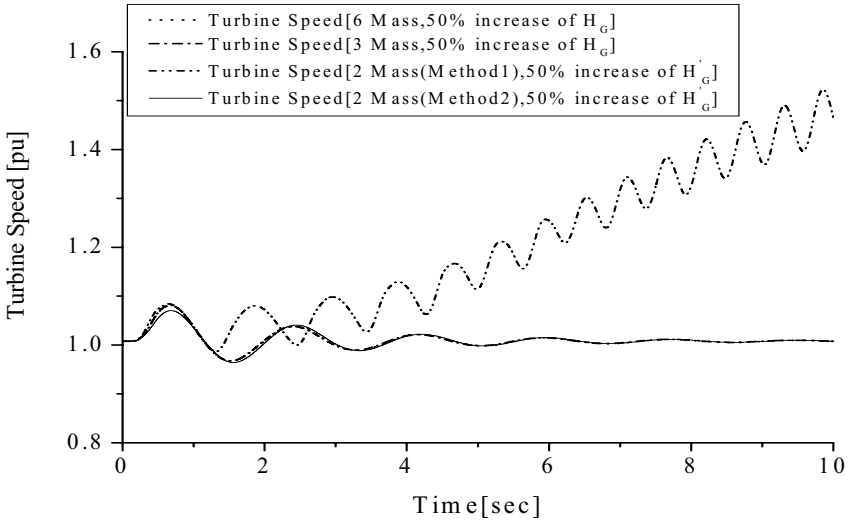

Fig. 2.25 Effect of the increased inertia constant of the generator on the turbine speed (Condition 2, 3LG, model system I)

b. Effect of Spring Constants

In this section, the effect of a spring constant on the transient stability of a WTGS is demonstrated using the six-mass, three-mass and two-mass drive train models. Here, the damping is neglected. The 3LG fault is considered to occur at point F of Fig. 2.14. First, the results of the transient characteristics of the six-mass drive

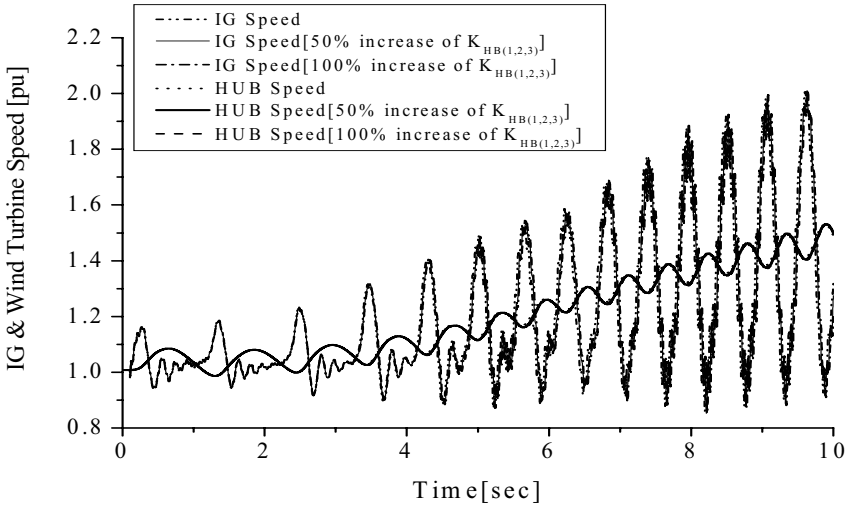

Fig. 2.26 Effect of the spring constant between the hub-blades of the six-mass model (Condition 2, 3LG, model system I)

train model are presented where the stiffness between the hub-blades, gearbox-generator, and hub-gearbox are increased by certain percentages from the original values as shown in Figs. 2.26, 2.27, and 2.28, respectively. It is seen from those figures that the stiffnesses between the hub-blades and gearbox-generator have a negligible effect on the transient stability of a WTGS. But the transient stability strongly depends on the spring constant between the hub-generator. In the three-mass drive train model, it is also seen that the spring constant between the

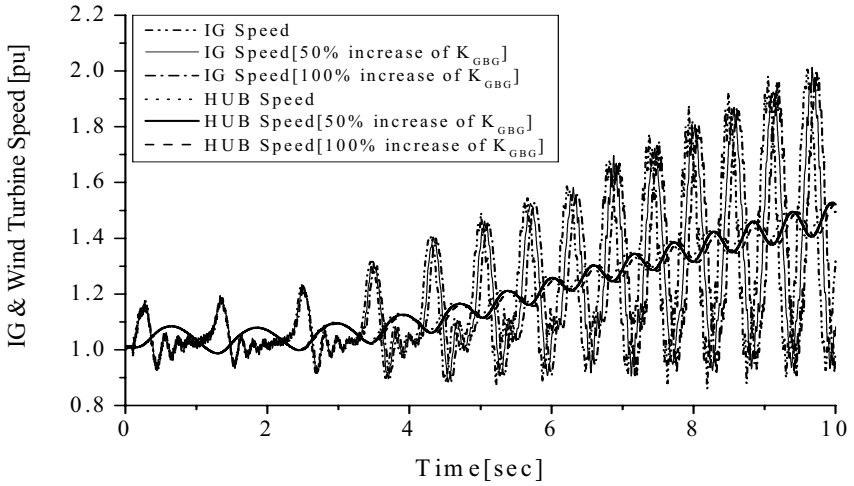

Fig. 2.27 Effect of the spring constant between the gearbox-generator of the six-mass model (Condition 2, 3LG, model system I)

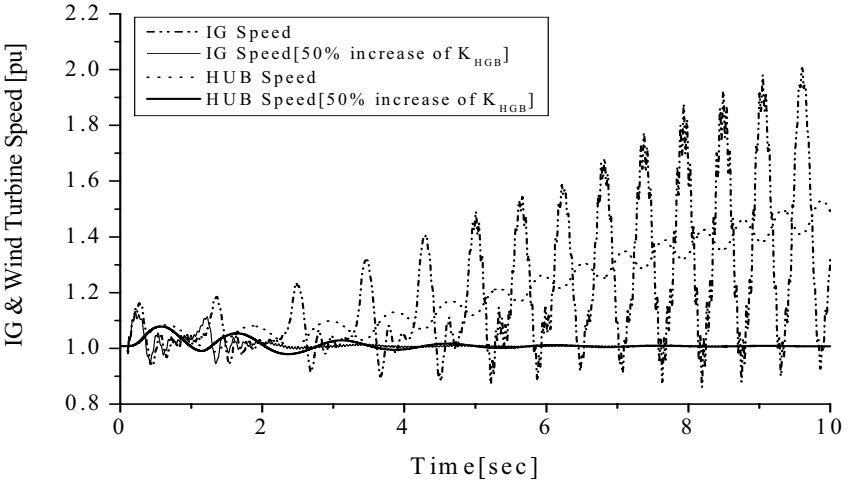

Fig. 2.28 Effect of the spring constant between the hub-gearbox of the six-mass model (Condition 2, 3LG, model system I)

gearbox-generator has almost no effect on stability, as shown in Fig. 2.29. Finally, the effect of the spring constant between the hub-gearbox for the six-mass and three-mass models and the effect of equivalent stiffness of the two-mass model are compared in Fig. 2.30 for a severe network disturbance in the model system. Moreover, these stiffnesses are increased by 50 % from the original values and their effects can be observed in Fig. 2.31. It is clear from Figs. 2.30 and 2.31 that the two-mass shaft model has almost the same transient characteristics as those of the six-mass and three-mass drive train models under a network disturbance.

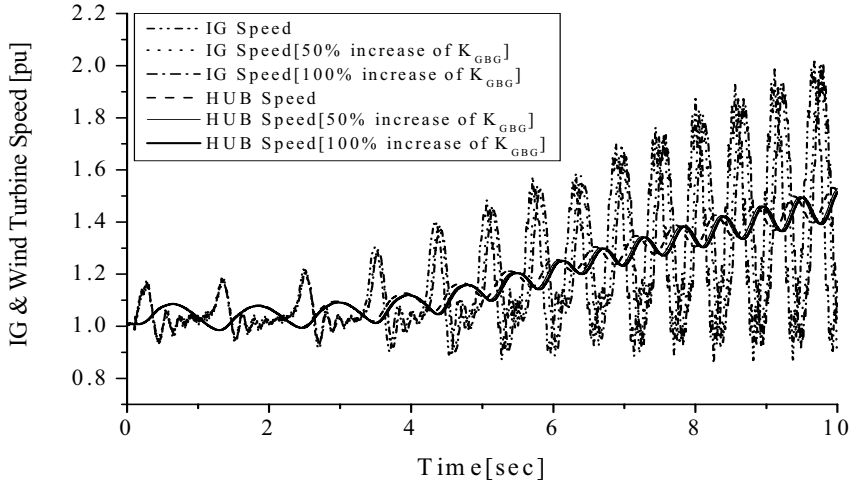

Fig. 2.29 Effect of the spring constant between the gearbox-generator of the three-mass model (Condition 2, 3LG, model system I)

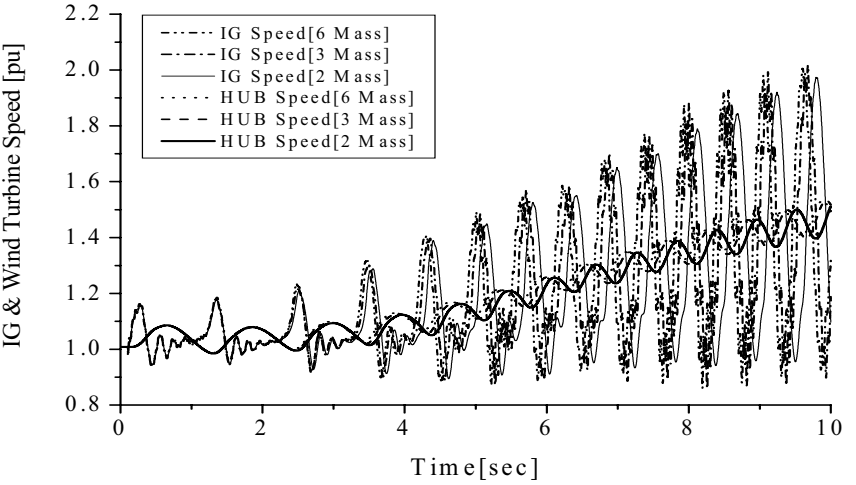

Fig. 2.30 Effect of the spring constant between the hub-gearbox of the six, three, and two mass models (Condition 2, 3LG, model system I)

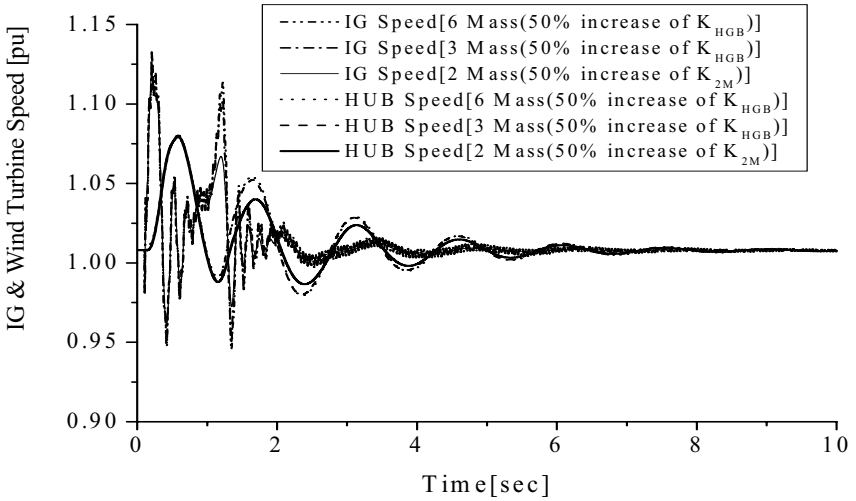

Fig. 2.31 Effect of the increased spring constant between the hub-gearbox of the six, three, and two mass models (Condition 2, 3LG, model system I)

c. Effect of Damping Constants

In this section, the effect of self and mutual damping of a drive train are analyzed using the six-mass, three-mass, and two-mass models under a severe network disturbance in the model system. The responses of the IG rotor and turbine speeds of the the six-mass model are shown in Figs. 2.32 and 2.33, respectively, where the damping constant is considered or disregarded. It is seen that both self and mutual

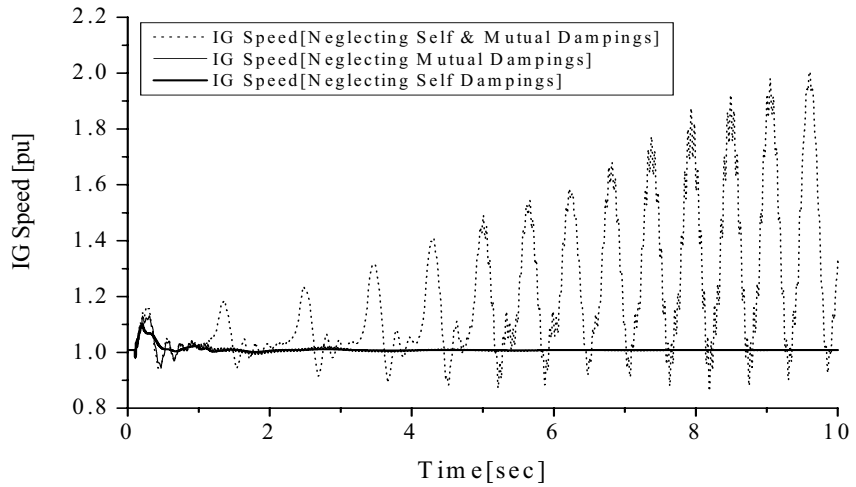

Fig. 2.32 Effect of the damping constants of the six-mass model on the generator speed (Condition 2, 3LG, model system I)

damping have significant effects on the transient stability of a WTGS, and among these two dampings, the mutual damping makes the WTGS transiently more stable. But in the three-mass model, it is not possible to consider the mutual damping between the hub and blades. In the two-mass model, only the mutual damping between the hub and gearbox is present. External damping elements represent torque

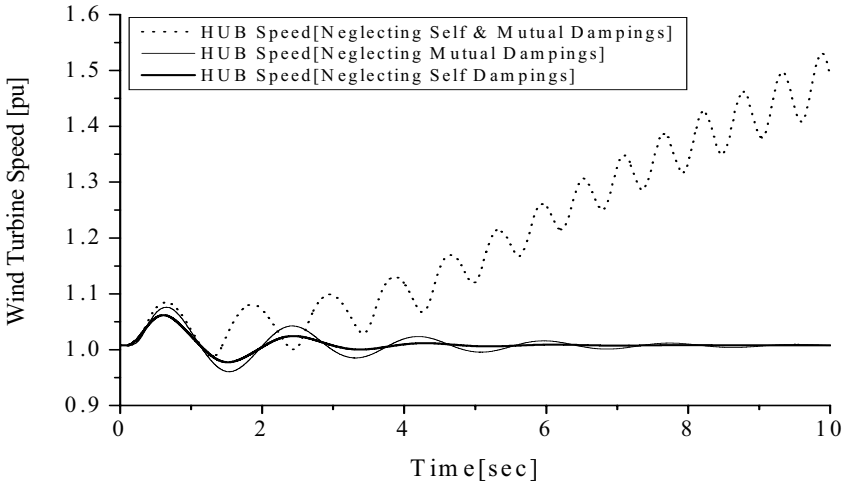

Fig. 2.33 Effect of the damping constants of the six-mass model on the turbine speed (Condition 2, 3LG, model system I)

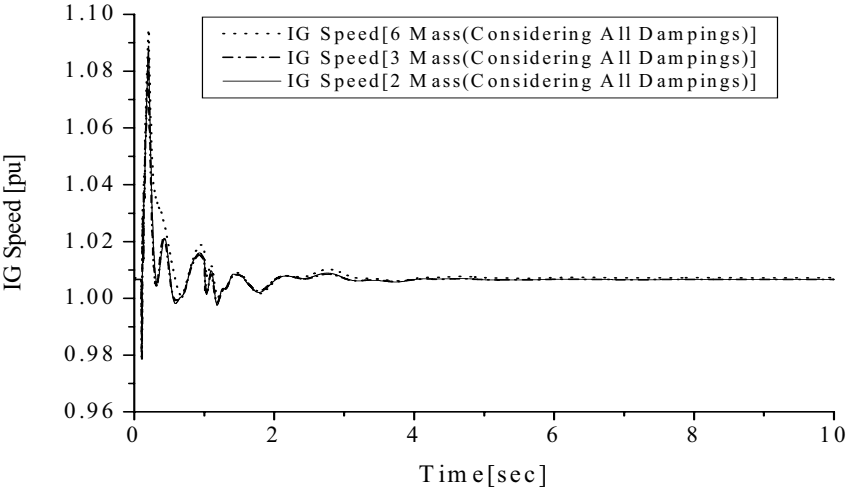

Fig. 2.34 Effect of the damping constants of the six, three, and two-mass models on the generator speed (Condition 2, 3LG, model system I)

losses. As the generator and gearbox masses are lumped together in the two-mass model, the self-damping of the individual elements is also lumped together. Finally, simulations have been carried out using the damping values shown in Table 2.4 and it is found that the two-mass, three-mass, and six-mass drive train models give almost the same results shown in Figs. 2.34 and 2.35.

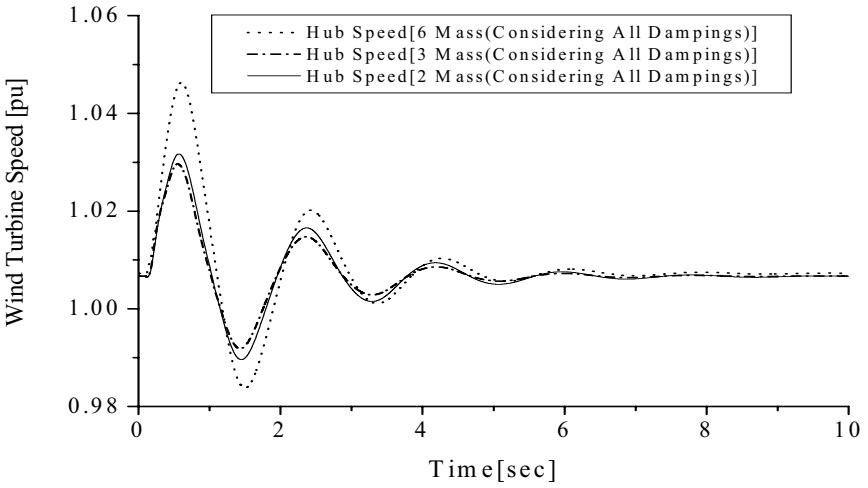

Fig. 2.35 Effect of the damping constants of the six, three, and two-mass models on the turbine speed (Condition 2, 3LG, model system I)

2.3.4.3.2 Fault Analysis

The transient stability of WTGS is analyzed again here using the six-mass, three-mass, and two-mass drive train models against different types of symmetrical and unsymmetrical faults in model system I. Drive train parameters are taken from Tables 2.4 and 2.5. The initial values at different IG output power levels can be obtained from the method described in [43]. The simulation results with and without considering the damping are shown briefly in Tables 2.6 and 2.7, where O and × represent stable and unstable situations of the WTGS, respectively. It is clear from the simulation results that in all cases the two-mass shaft model give the same results as those of the three-mass and six-mass drive train models.

Table 2.6 Transient stability results for two-mass, three-mass and six-mass models (neglecting all types of damping, Condition 3)

IG POWER (MW)	1LG fault			2LS fault			2LG fault			3LG fault		
	2M	3M	6M	2M	3M	6M	2M	3M	6M	2M	3M	6M
50	O	O	O	O	O	O	×	×	×	×	×	×
44	O	O	O	O	O	O	×	×	×	×	×	×
43	O	O	O	O	O	O	O	O	O	×	×	×
40	O	O	O	O	O	O	O	O	O	×	×	×
39	O	O	O	O	O	O	O	O	O	O	O	O

Table 2.7 Transient stability results for two-mass, three-mass and six-mass models (considering all types of damping, Condition 3)

IG POWER (MW)	1LG fault			2LS fault			2LG fault			3LG fault		
	2M	3M	6M	2M	3M	6M	2M	3M	6M	2M	3M	6M
50	O	O	O	O	O	O	O	O	O	O	O	O

2.3.4.4 Comparison Using Model System II

Other simulation results using model system II are shown here, in which longer fault clearing times and circuit breaker reclosing times are used. A fault occurs at 0.1 sec, the circuit breakers (CB) on the faulted line are opened at 0.22 sec and at 1.22 sec, are reclosed. Table 2.3 shows the initial values used in the simulation. A 3LG fault is considered to occur at fault point F of Fig. 2.17. The responses of the IG rotor and the turbine hub speeds for Conditions 4 and 5 are shown in Figs. 2.36 and 2.37, respectively. It is seen that all types of drive train models show similar characteristics for both Condition 4 and 5. Therefore, it is clear that the three drive train models show similar transient characteristics for both stable and unstable conditions of a WTGS. Some other simulation results are presented in Figs. 2.38 and 2.39 for a 2LG fault using Condition 4, in which the transformer near the induction generator is grounded or ungrounded, respectively. In these results, the six, three, and two mass drive train models also show the same transient characteristics during a network disturbance.

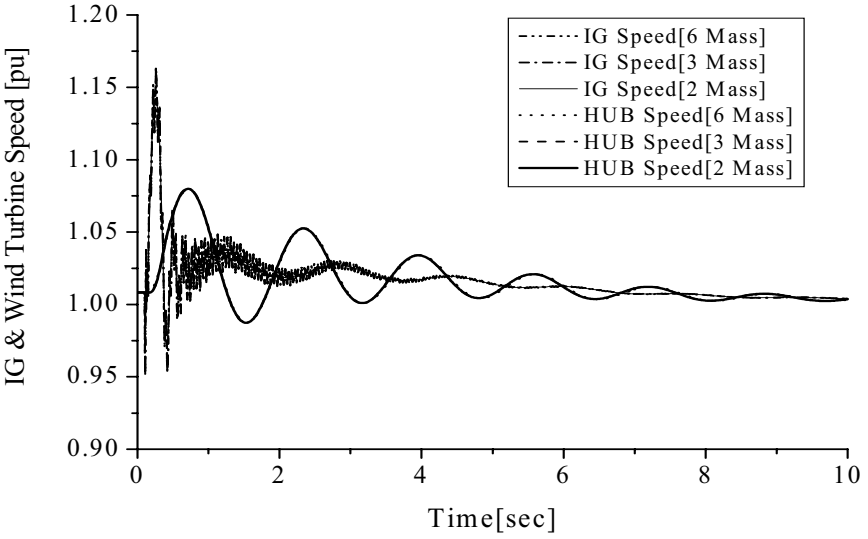

Fig. 2.36 Speed responses of the six, three, and two-mass models (Condition 4, 3LG, model system II)

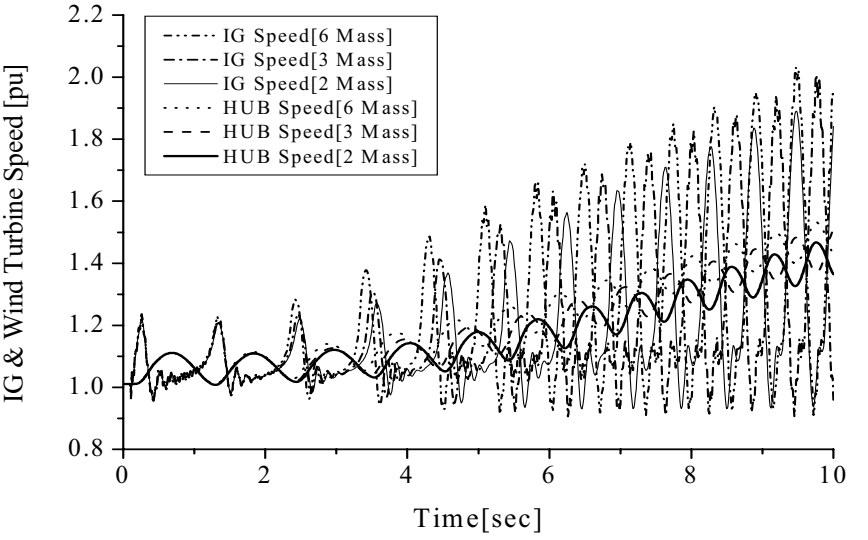

Fig. 2.37 Speed responses of the six, three, and two-mass models (Condition 5, 3LG, model system II)

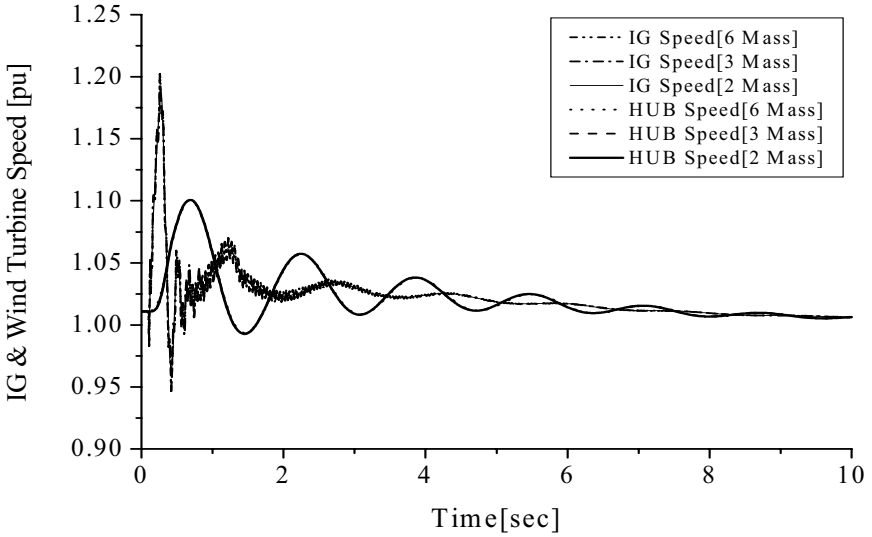

Fig. 2.38 Speed responses of the six, three, and two-mass models (Condition 4, 2LG, model system II, transformer grounded)

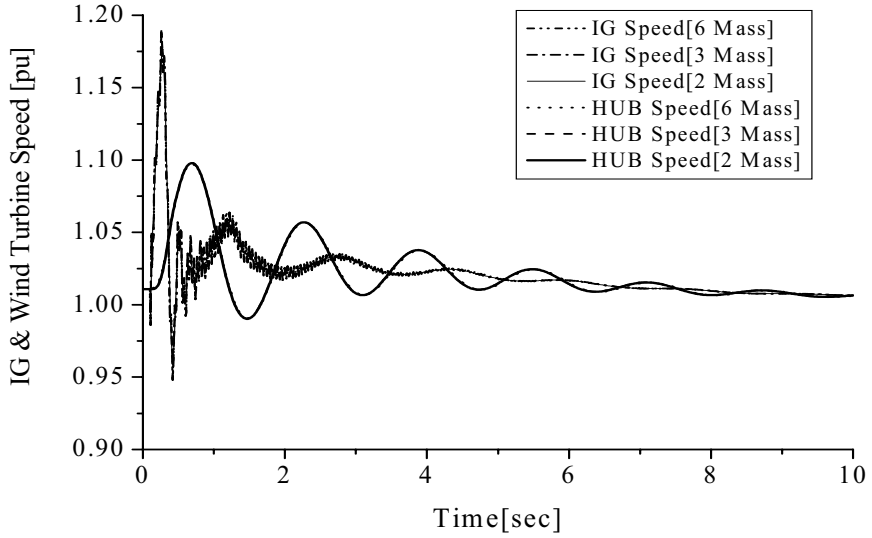

Fig. 2.39 Speed responses of the six, three, and two-mass models (Condition 4, 2LG, model system II, transformer ungrounded)

2.4 Variable Speed WTGS

Another commercial trend of a wind power generation is in using variable speed wind turbine (VSWT) driving a doubly fed induction generator (DFIG), wound field synchronous generator (WFSG) or permanent magnet synchronous generator (PMSG). The main advantage of variable speed operation is that more energy can be generated for a specific wind speed regime. Although the electrical efficiency decreases due to the losses in the power electronic converters that are essential for variable speed operation, the aerodynamic efficiency increases due to variable speed operation [119]. The aerodynamic efficiency gain can exceed the electrical efficiency loss, resulting in a higher overall efficiency [127, 128]. In addition, the mechanical stress is less because the rotor acts as a flywheel (storing energy temporarily as a buffer), reducing the drive train torque variations. Noise problems are reduced as well because the turbine runs at low speed. The main drawback of variable speed generating systems is that they are more expensive. However, using a variable speed generating system can also give major savings in other subsystems of the turbine such as lighter foundations in offshore applications, limiting the overall cost increase.

2.4.1 Variable Speed Topological Overview

The currently available variable speed wind turbine generator system topologies are shown in Fig. 2.40. To allow variable speed operation, the mechanical rotor speed and the electrical frequency of the grid must be decoupled. Therefore, a power electronic converter is used in a variable speed wind turbine generator system. In the doubly fed induction generator, a back-to-back voltage source converter feeds the three-phase rotor winding. In this way, the mechanical and electrical rotor frequency are decoupled, and the electrical stator and rotor frequencies can be matched independently of the mechanical rotor speed. In the direct drive synchronous generator system (PMSG or WFSG), the generator is completely decoupled from the grid by a frequency converter. The grid side of this converter is a voltage source converter, i.e., an IGBT (insulated gate bipolar transistor) bridge. The generator side can be either a voltage source converter or a diode rectifier.

The generator is excited using either an excitation winding (in the case of a WFSG) or permanent magnets (in the case of PMSG). In addition to these three mainstream generating systems, there are some other varieties, as explained in [119, 120].

One that must be mentioned here is the semi-variable speed system. In a semi-variable speed turbine, a winding type induction generator of which the rotor resistance can be changed by power electronics is used. By changing the rotor

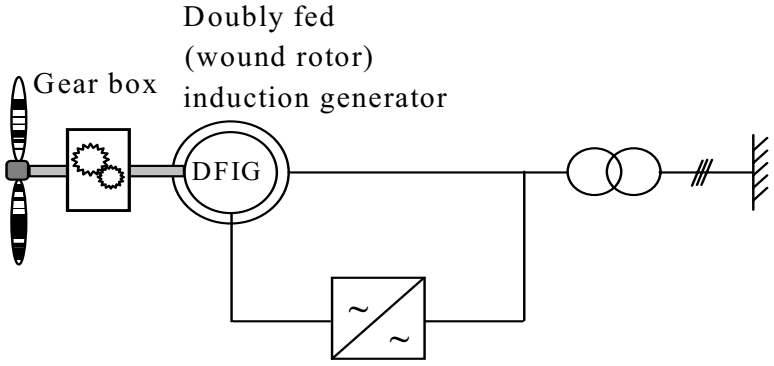

(a) Schematic diagram of VSWT-DFIG

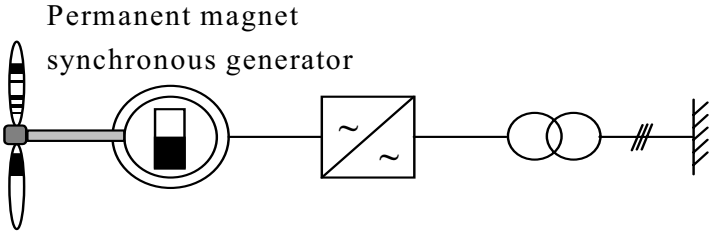

(b) Schematic diagram of direct drive VSWT-PMSG

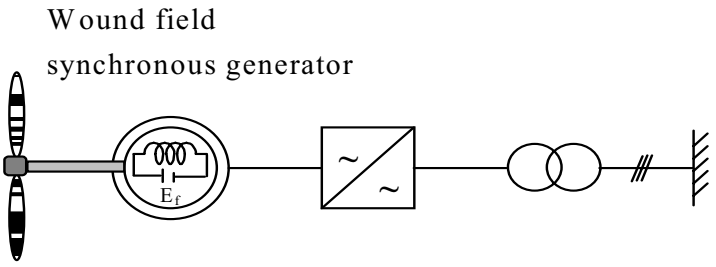

(c) Schematic diagram of direct drive VSWT-WFSG

Fig. 2.40 Commercially available variable speed wind turbine generator systems

resistance, the torque/speed characteristic of the generator is shifted, and about a 10 % rotor speed decrease from the nominal rotor speed is possible. In this generating system, a limited variable speed capability is achieved at relatively low cost.

Other variations are a squirrel cage induction generator and a conventional synchronous generator connected to the wind turbine through a gearbox and to the grid by a power electronics converter of the full generator rating.

2.4.2 Variable Speed Wind Turbine Characteristics

To calculate Cp for the given values of β and λ, the following numerical approximations [34, 120] have been used in this study.

$$\lambda = \frac{\omega_r R}{V_w} \tag{2.28a}$$

$$\lambda_i = \frac{1}{\frac{1}{\lambda + 0.02\beta} - \frac{0.03}{\beta^3 + 1}} \tag{2.28b}$$

$$C_p(\lambda, \beta) = 0.73\left[\frac{151}{\lambda_i} - 0.58\beta - 0.002\beta^{2.14} - 13.2\right] e^{\frac{-18.4}{\lambda_i}} \tag{2.28c}$$

For a VSWT, generated active power depends on the power coefficient, C_p, which is related to the proportion of power extracted from the wind hitting the wind turbine blades. From Eq. 2.28c, the optimum values of tip speed ratio and power coefficient are chosen as 5.9 and 0.44 respectively. For each instantaneous wind speed of a VSWT, there is a specific turbine rotational speed, that corresponds to the maximum active power from the wind generator. In this way, the maximum power point tracking (MPPT) for each wind speed, increases the energy generation in a VSWT.

In this book, the 2.5 MW wind turbine with a rotor diameter of 84 m is considered. Its power coefficient curve with MPPT is shown in Fig. 2.41, from which it can be seen that, for any particular wind speed, there is a rotational speed, ω_r, that corresponds to the maximum power, P_{max}.

When the wind speed changes, the rotational speed is controlled to follow the maximum power point trajectory. Note here that precise measurement of wind

speed is difficult. Therefore, it is better to calculate the maximum power, P_{max}, without measuring wind speed, as shown below:

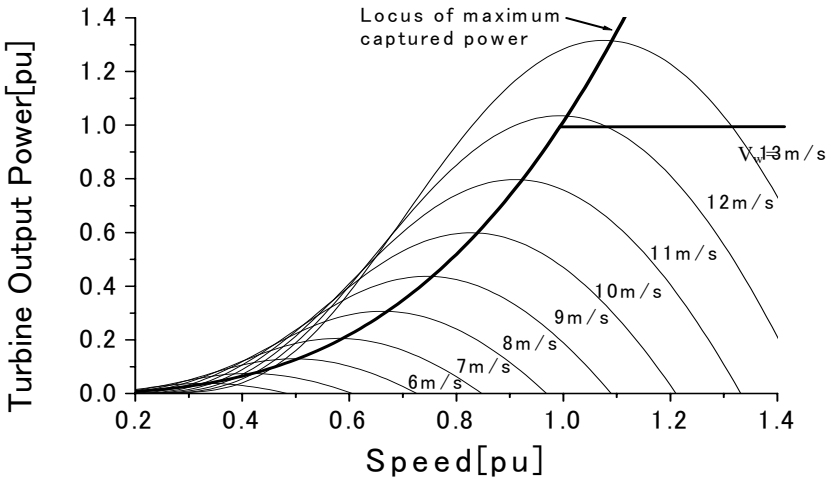

Fig. 2.41 Turbine characteristic with maximum power point tracking

$$P_{max} = 0.5\rho\pi R^2 \left(\frac{\omega_r R}{\lambda_{opt}} \right)^3 C_{p\_opt} \tag{2.29}$$

From Eq. 2.29, it is clear that the maximum power generated is proportional to the cube of the rotational speed as shown below:

$$P_{max} \propto \omega_r^3 \tag{2.30}$$

2.4.3 Influence of Drive Train Modeling on Variable Speed WTGS

For a fixed speed WTGS, detailed drive train dynamics might be considered, especially in transient analysis, as mentioned in Sect. 2.3.3. In a VSWT, however, the drive train properties have almost no effect on the grid side characteristics due to the decoupling effect of the power electronic converter [34]. Therefore, in the

analyses of variable speed wind turbine generator system, the simple one-mass lumped model is considered in this book.

2.5 Chapter Summary

In this chapter, the basic theory of mechanical power extraction from wind is described briefly. Then fixed and variable speed wind turbine systems are explained in detail. The initial value calculation method for a power system including a WTGS, is also described.

Then emphasis is given to the drive train modeling of a fixed-speed WTGS. Three different types of drive train models are presented, and a comparative study is carried out among those models. A detailed transformation methodology from the six-mass to two-mass drive train models is presented, which can be used in simulation analysis with reasonable accuracy. By using the transformation procedure the inertia constants, spring constants, the self damping of individual masses and mutual damping of adjacent masses of the six-mass drive train model can be converted to reduced order models. The effects of drive train parameters, such as inertia constants, spring constants, and damping constants are examined for the above mentioned three-types of drive train models. It is proved that the two-mass drive train model of a WTGS is sufficient enough for the transient stability analysis of a fixed speed WTGS. The commercially available fixed and variable speed WTGS topologies are also shown in this chapter.

http://www.springer.com/978-1-84800-315-6

Stability Augmentation of a Grid-connected Wind Farm

Muyeen, S.M.; Tamura, J.; Murata, T.

2009, XIV, 248 p., Hardcover
ISBN: 978-1-84800-315-6